PERGAMON

International Journal of Solids and Structures 38 (2001) 577–604

INTERNATIONAL JOURNAL OF SOLIDS and STRUCTURES

www.elsevier.com/locate/ijsolstr

Phenomenological modeling and numerical simulation of different modes of creep damage evolution

E. Bellenger *, P. Bussy

Université de Picardie Jules Verne-LMCAO, IUT de l'Aisne, 48 Rue d'Ostende, F-02100 Saint-Quentin, France

Received 10 March 1999

Abstract

This paper deals with a numerical analysis of creep components until failure. We will take an interest in the macroscopic modeling of the creep curves with its three stages based on the irreversible thermodynamics theory with internal variables. A "unified" viscoplastic model is used to describe primary and secondary creep behaviors, and the tertiary creep description is based on the introduction of a scalar damage variable and the nonlinear effects of changes in geometry. Therefore, viscoplastic damage models in nonlinear geometry are defined in order to describe different modes of creep damage development. The numerical properties of the models allow us to obtain a different crack growth development, in order to know the post-critical behavior and the damage development until failure. The numerical treatment uses the finite element method and the large time increment method in a version adapted to solve nonlinear problems with geometrical nonlinearities, in order to obtain a rapid creep life assessment.

Keywords: Creep damage descriptions; Viscoplasticity; Nonlinear geometry; Constitutive equations; Computation; Large time increment method

1. Introduction

In different industries, many engineering components such as conventional and nuclear power plants, chemical plants, aeroengines and so on, operate at temperatures high enough for creep to be an important design consideration. The failure of components operating at elevated temperatures can have catastrophic effects. Therefore, an inelastic stress analysis in the creep range is now seen as a normal procedure in component assessment. However, the engineer is not usually interested in the complete solution of a structural problem. In most cases, the solution is performed to allow structural assessment in terms of functional criteria which concern critical positions. Such positions may be predetermined, if criteria concern displacement (the tip of a blade touching a turbine casing). Most often, it is a matter of creep damage and creep life assessment when the critical positions need not be known in advance.

* Corresponding author. Tel.: +33-3-23-50-36-95; fax: +33-3-23-50-36-95.
E-mail address: emmanuel.bellenger@insset.u-picardie.fr (E. Bellenger).

0020-7683/01/$ - see front matter
PII: S0020-7683(00)00042-1

If numerical modeling of primary and secondary creep phases does not usually present any problems, it is not so with the tertiary creep period which will lead to failure and which is a determinant for creep life assessment. In order to describe primary and secondary creep behaviors, a "unified" viscoplastic model is used (Chaboche and Nouailhas, 1989). The tertiary creep description is based on the introduction of a scalar damage continuous variable (Kachanov, 1958). In addition to the influence of damage on the strain rate, the nonlinear effects of large changes in geometry may also significantly contribute to tertiary creep. Indeed, the experimental data on the creep rupture phenomenon allow us to distinguish two modes of fracture, which depend on the stress level and the temperature of the test (Skrzypek, 1993). The regimes and modes of growth of intergranular cavities by the combination of diffusional flow and creep deformation at different levels of stress and temperature have been studied extensively by many investigators. These developments have been reviewed by Argon (1982). Experiments on alloys with different microstructures have identified two limiting types of damage morphology. One limiting type is ductile solids, and the another is less ductile (brittle), but much more creep resistant.

In order to describe the above creep rupture phenomena, we will define a viscoplastic damage model for brittle rupture, a viscoplastic viscodamage model in nonlinear geometry for ductile rupture and a viscoplastic damage model in nonlinear geometry for combined ductile–brittle rupture.

The finite element method codes, generally use Newton–Raphson methods for solving nonlinear problems. These methods are incremental in time and iterative on each increment. These are costlier when nonlinearities accumulate. This is the case for our problem which involves several nonlinearities. Unlike classical incremental techniques, the large time increment (LATIN) method that is used in this paper, enables these problems to be simulated without proceeding by small increments. This method was first introduced by Ladevèze (1985) in the context of structural mechanics. We have developed a version, which is applicable to nonlinear problems with geometrical nonlinearities (Bellenger, 1998b). This numerical method does not divide the loading into small increments. The iterative process gives for each iteration a new estimation solution for large loading increment. This strategy makes it easy to reach swiftly the tertiary creep period.

In the following, after a presentation of the general thermodynamical framework, the different models are introduced. These models have been implemented in our finite element code. We will show a rupture time assessment using different creep rupture theories. We will describe different modes of damage development and their dependences on the level of stress, and we will verify the very different early crack growth behavior exhibited by different structures. For the numerical resolution, the LATIN method appears suitable to the treatment of structures undergoing creep conditions. Indeed, this method can handle large time increments during primary and secondary creep phases to reach swiftly the tertiary creep period which involves most nonlinearities and which leads to failure. The version of the LATIN method developed in this work will be presented.

2. Constitutive equations

In this work, the phenomenological approach is chosen by using an internal variable to describe the consequences of damage evolution on the elastic properties as well as on the plastic or viscoplastic flow properties of the material. The scalar damage variable D used by Lemaitre and Chaboche (1978) and many other authors is interpreted as the effective area reduction caused by the distributed microscopic cracks and cavities due to material damage (Lemaitre, 1984; Krajcinovic, 1989). Creep damage through the use of an internal state variable was modeled phenomenologically first for the design application by Kachanov (1958) and Rabotnov (1968). They introduced a scalar damage parameter D into creep constitutive relations. The evolution of this parameter which increase from zero at the start life to unity at failure, was linked to creep strain in a functional dependence on stress that could be fitted to specific experimental results. This ap-

proach was later modified by Leckie and Hayhurst (1977) and incorporated into a general finite element method computer code to solve creep damage distribution problems (Saanouni et al., 1986; Murakami and Ohno, 1988). This formulation which can represent primary creep as well as the secondary and tertiary creep are assumed to apply with instantaneous values of time (measured from the first instant of creep), so that time is employed as an internal variable. Although this is incorrect in principle, reasonable results may often be obtained if the stress varies slowly. This method is widely used for its convenience. However, in this approach, during finite element resolution, the elastic modulus is assumed to be independent of damage and remains fixed at its initial value. In practice, most creep analyses are based on the creep curves of standard test data in a "superposition" treatment with a single internal variable taken as either time (fundamentally incorrect but useful in some circumstances) or as equivalent creep strain (Wilshire and Evans, 1994; Harrison and Homewood, 1994). The latter is quite satisfactory, if stress states do not vary too greatly or too rapidly during creep, at least for primary and secondary behaviors. This, however, may cease to be true if the uniaxial law is employed in the tertiary range as the tertiary creep is known often to vary significantly with stress.

Backstress models (primary and secondary creep) are now available, often within "unified" approach, for the treatment of more variable stress states. Therefore, in this work, backstress model within "unified" formulation will be used for the numerical simulation of primary and secondary creep periods associated with a scalar damage variable and nonlinear geometrical effects for the tertiary creep description. In "unified" models, the common features are the viscoplastic potential and the definition of the viscoplastic flow from the normality rule. In the case of initially isotropic material, the elastic domain is defined by a sphere in deviatoric stress space. A "unified" formulation as in Robinson (1978) and Chaboche and Nouailhas (1989), which is sometimes known as viscoplastic is used. A time dependent yield function is introduced, and the stress may depart from the elastic domain.

2.1. General framework

The modeling of processes associated with viscoplasticity in the framework of a continuum mechanics approach has led to many specific theories that incorporate viscoplastic flow, hardening and damage effects. Dynamic recovery effects, static recovery effects (time recovery of hardening) and aging effects are not considered in this work. Moreover, these constitutive equations are generally built into a thermodynamics framework with two potentials (Germain, 1972): the state potential (or thermodynamics potential that gives the state laws), and the dissipation potential that gives evolution laws for state variables associated to irreversible processes, through the generalized normality assumption (giving rise to the notion of "standard generalized materials"). We consider the Helmholtz free energy as the thermodynamics potential. This presentation assumes elasticity coupled with isotropic damage as an isothermal process. We will consider only isotropic hardening. The state variables are the elastic strain tensor ε_e. The total strain ε can expressed as the sum of the elastic and the viscoplastic strain, ε_e and ε_{vp}.

In the past, a large number of models have been developed in order to allow numerical simulations of structural damage. The implementation of these models in finite element codes is difficult, because it leads to unstable calculations. Convergence becomes impossible after limiting points. This problem results from the bad modelization of nonconvex free energy. Therefore, we propose to use for the above models, a convex elastic damage model (Benkrid et al., 1994a), stable to "standard generalized materials" (Halphen and Nguyen, 1975) in its formulation for small transformations. The extension in nonlinear geometry is carried out in the kinematic context of the corotational model (Ladevèze, 1981). The choice of a damage convex written with the stress tensor ensures stability. Many numerical results have been presented in Benkrid (1994b) and Abdali et al. (1996), in order to show stable calculations. This model can easily be implemented in industrial codes to give damage zone and the maximal loading. This model has been extended to viscoplasticity and nonlinear geometry (Bellenger and Bussy, 1998a). In the following, we will

begin to present constitutive laws in small perturbations before presenting their extensions in nonlinear geometry.

In this study, the internal state variables associated with irreversible processes are the following:

- p is the scalar isotropic hardening variable for viscoplastic deformation. Restricting our consideration to simple loading histories, we will employ an isotropic yield surface by using the Von Mises yield condition and the Prandtl–Reuss behavior law, p is the accumulated viscoplastic strain: $p = \int_0^t \left[\frac{2}{3}\dot{\varepsilon}_{vp}(\tau) : \dot{\varepsilon}_{vp}(\tau)\right]^{1/2} d\tau$.
- X is the scalar damage variable describing the current state of damage.

In this work, we will introduce a new scalar damage variable X related to the usual damage variable D bounded by 0 and 1:

$$X = \frac{D}{1-D} \Rightarrow 1 - D = \frac{1}{1+X}. \tag{1}$$

ΔD must verify the condition $D + \Delta D < 1$, then X is not bounded which avoids numerical integrations problems. X takes values within the range 0 (for virgin material) to ∞ (corresponding to complete failure).

We assume some uncouplings between the various state variables and the free energy. Thus, the Helmholtz free energy per unit volume $\rho\psi$ can be expressed as follows:

$$\rho\psi(\varepsilon_e, X, p) = \rho\psi_e(\varepsilon_e, X) + \rho\psi_{vp}(p) + \rho\psi_X(X), \tag{2}$$

where $\rho\psi_e(\varepsilon_e, X)$ is the elastic strain energy incorporating the effects of the damage on the elastic response of the material, whereas $\rho\psi_{vp}(p)$ and $\rho\psi_X(X)$ are the free energies induced by isotropic hardening and damage development, respectively. ρ is the material density.

By differentiating Eq. (2) with respect to time and substituting the resulting expression into the Clausius–Duhem inequality, we have the following elastic constitutive equation as a result of nonnegative requirement of entropy production:

$$\sigma = \rho\frac{\partial\psi}{\partial\varepsilon_e} = \rho\frac{\partial\psi_e}{\partial\varepsilon_e}, \tag{3}$$

where σ is the Cauchy stress tensor.

We will represent the thermodynamics conjugate forces Y and R corresponding to X and p, respectively, as follows:

$$R = \rho\frac{\partial\psi}{\partial p} = \rho\frac{\partial\psi_{vp}}{\partial p}, \qquad Y = \rho\frac{\partial\psi}{\partial X} = \rho\frac{\partial\psi_e}{\partial X} + \rho\frac{\partial\psi_X}{\partial X}. \tag{4}$$

In the initial undamaged state, the elastic behavior is assumed to be isotropic and linear and thus the function $\rho\psi_e(\varepsilon_e)$ is quadratic in ε_e. In order to take into account the effects of damage on the elastic response, X is introduced into $\rho\psi_e$ as follows (Lemaitre and Chaboche, 1985):

$$\rho\psi_e(\varepsilon_e, X) = \frac{1}{2}\frac{\mathrm{tr}(\varepsilon_e C_e \varepsilon_e)}{1+X} = \frac{1}{2}\frac{\lambda}{1+X}[\mathrm{tr}(\varepsilon_e)]^2 + \frac{\mu}{1+X}\left[\mathrm{tr}(\varepsilon_e^2)\right], \tag{5}$$

where C_e is the symmetric fourth-order tensor of elastic properties, λ and μ are the classic Lame's constants, tr(.) is the trace of a tensor. $\rho\psi_{vp}(p)$ and $\rho\psi_X(X)$ are convex functions of their argument and contain the origin $\rho\psi_{vp}(0) = \rho\psi_X(0) = 0$.

According to the thermodynamics formulation discussed above, the elastic constitutive equation of the damage material can be obtained by the use of Eqs. (3) and (5), and leads to

$$\sigma = \rho\frac{\partial\psi_e}{\partial\varepsilon_e} = \frac{C_e}{1+X}\varepsilon_e. \tag{6}$$

The conjugate force corresponding to the internal state variable p is derived from Eq. (4). In order to describe the primary creep period in which the creep rate continuously decelerates followed by a secondary stage during which a minimum steady creep rate is maintained, we use for R, the following form:

$$R = \rho \frac{\partial \psi_{\mathrm{vp}}}{\partial p} = Q(1 - \exp(-bp)), \tag{7}$$

where Q and b are material constants.

For a fixed applied stress, such form predicts that R changes from zero to an asymptotic value Q. Without damage, Eq. (21) allows us to have $\dot{\varepsilon}_{\mathrm{vp}}$, which varies from an initial to a lower steady value. b is the saturation speed of R. Thus, we have

$$\rho \psi_{\mathrm{vp}}(p) = Q\left(p + \frac{1}{b} \exp(-bp) - \frac{1}{b} \right). \tag{8}$$

The conjugate force corresponding to the internal state variable X is derived from Eq. (4):

$$Y = \frac{\partial \rho \psi}{\partial X} = -\frac{1}{2} \mathrm{tr}\left(\varepsilon_{\mathrm{e}} \frac{C_{\mathrm{e}}}{(1+X)^2} \varepsilon_{\mathrm{e}} \right) + Z(X). \tag{9}$$

$$Z(X) = \rho \frac{\partial \psi_X}{\partial X}. \tag{10}$$

From Eqs. (6) and (9) we can write Y as follows:

$$Y = -\tfrac{1}{2}\mathrm{tr}(\sigma C e^{-1} \sigma) + Z(X). \tag{11}$$

The choice of the variable X has a share in the numerical stability of the damage model, with the choice of the Helmholtz free energy written in Eq. (2).

2.1.1. Dissipation potential

The second principle of thermodynamics requires to write and verify the Clausius–Duhem inequality. From Eqs. (3) and (4), this inequality takes the following form:

$$\Phi = \mathrm{tr}(\sigma \dot{\varepsilon}_{\mathrm{vp}}) - R\dot{p} - Y\dot{X} \geqslant 0, \tag{12}$$

where Φ represents the intrinsic dissipation.

The dissipation of viscoplastic deformation in polycrystalline materials is mainly produced by dislocation motion under stress, whereas the dissipation of damage is governed by the release of an internal energy due to the development of macroscopic cavities. In order to satisfy Eq. (12), we assume damage and viscoplastic processes are independent processes. Therefore, Eq. (12) can be written as the sum of two parts:

$$\Phi_{\mathrm{vp}} = \mathrm{tr}(\sigma \dot{\varepsilon}_{\mathrm{vp}}) - R\dot{p} \geqslant 0 \ \text{(viscoplastic dissipation)}, \quad \Phi_X = -Y\dot{X} \geqslant 0 \ \text{(damage dissipation)}. \tag{13}$$

Therefore, we can represent these dissipation mechanisms by two different potential functions: a viscoplastic potential φ^*_{vp}, and a damage potential φ^*_X. Then, the total dissipation potential is given as the sum of these two parts:

$$\varphi^*(\sigma, R, Y) = \varphi^*_{\mathrm{vp}}(\sigma, R) + \varphi^*_X(Y). \tag{14}$$

The laws of viscoplasticity with damage are derived from this potential through the normality assumption. They are defined below:

$$\dot{\varepsilon}_{\mathrm{vp}} = \frac{\partial \varphi^*_{\mathrm{vp}}}{\partial \sigma}, \tag{15}$$

$$\dot{p} = -\frac{\partial \varphi^*_{\mathrm{vp}}}{\partial R}, \tag{16}$$

$$\dot{X} = -\frac{\partial \varphi^*_{X}}{\partial Y}. \tag{17}$$

Clearly, if φ^*_{vp} and φ^*_X are positive convex functions of their arguments and contain the origin ($\varphi^*_{\mathrm{vp}}(0,0) = \varphi^*_X(0) = 0$), the second principle is automatically verified. Here, the intrinsic dissipation takes the following form:

$$\Phi_{\mathrm{vp}} = \left[\sigma : \frac{\partial \varphi^*_{\mathrm{vp}}}{\partial \sigma} + R\frac{\partial \varphi^*_{\mathrm{vp}}}{\partial R}\right] \geqslant 0 \quad \text{and} \quad \Phi_X = Y\frac{\partial \varphi^*_X}{\partial Y} \geqslant 0. \tag{18}$$

In this study, the time dependent viscoplastic behavior is carried out by using Chaboche's viscoplastic constitutive equation (Lemaitre, 1984). The author introduces the concept of the elastic domain described in the stress space as

$$f_{\mathrm{vp}}(\sigma, R(p)) = \sigma_{\mathrm{eq}} - R(p) - R_0 \leqslant 0, \tag{19}$$

where R is the scalar variable (or drag stress) given by Eq. (4) responsible for the isotropic hardening effect. R describes the size of the elastic domain. σ_{eq} is the Von Mises equivalent stress. $\sigma_{\mathrm{eq}} = \sqrt{\frac{3}{2}\mathrm{tr}(ss)}$ and s is the deviatoric part of the Cauchy stress tensor. $R_0 \geqslant 0$ denotes the initial viscoplastic hardening limit.

In plasticity, the associated flow rule requires the orthogonality of $\dot{\varepsilon}_{\mathrm{vp}}$ to the yield surface at the point σ that belongs to the surface $f_{\mathrm{vp}} = 0$. In viscoplasticity, σ lies outside the actual yield surface, $f_{\mathrm{vp}} > 0$. Rice (1970) suggested the existence of the viscoplastic potential as the extension of f_{vp} beyond the yield surface expressed as a power function of f_{vp} (often called the overstress or the viscous stress).

$$\varphi^*_{\mathrm{vp}} = \frac{K}{n+1}\left\langle \frac{f_{\mathrm{vp}}}{K} \right\rangle_+^{n+1}, \tag{20}$$

where K and n are material parameters, $\langle . \rangle_+$ denotes the positive part.

The viscoplastic potential of Eq. (20) together with Eqs. (15) and (16) furnish the evolution equations for viscoplastic strain $\varepsilon_{\mathrm{vp}}$ and the isotropic hardening p as follows:

$$\dot{\varepsilon}_{\mathrm{vp}} = \frac{\partial \varphi^*_{\mathrm{vp}}}{\partial \sigma} = \frac{3}{2}\frac{s}{\sigma_{\mathrm{eq}}}\left\langle \frac{f_{\mathrm{vp}}}{K} \right\rangle_+^{n}, \tag{21}$$

$$\dot{p} = -\frac{\partial \varphi^*_{\mathrm{vp}}}{\partial R} = \left\langle \frac{f_{\mathrm{vp}}}{K} \right\rangle_+^{n}. \tag{22}$$

In viscoplasticity, we obtain an explicit form for $\dot{p}$ and $\dot{\varepsilon}_{\mathrm{vp}}$.

The choice of φ^*_X and the coupling with geometrical nonlinearities (as the case may be) will allow us to describe the tertiary creep period and different modes of creep damage evolution as defined below.

2.2. Phenomenological modeling of creep damage

For structural purposes, failure in a creeping part can be considered to result from different mechanisms and phenomena. Experiments have identified two limiting modes of fracture, which depend on the stress level and the temperature of the test:

A ductile (or viscous) fracture is preceded by a reduction of the cross-sectional area due to large creep strains essentially caused by a slip deformation within the grains. The growth and coalescence of cavities in these materials is quite unhomogeneous. These subsequently grow further by the creep deformation,

to interact with each other and eventually result in overall fracture (Chen and Argon, 1981; Don and Majumbar, 1986). The ductile rupture mechanism occurs at high stress levels and low temperature regimes.

A brittle or intergranular fracture is caused by the deterioration of material due to the formation of voids at grain boundaries. This fracture mechanism results in the growth of voids and the corresponding reduction of effective cross-sectional area below a critical value. The intergranular cavitation process in these alloys is more homogeneous and leads to overall fracture without the intermediate formation of an appreciable density of microcracks. The brittle fracture mechanism occurs at low stress levels and high temperatures. The overall geometric effect is not observed as creep strains are small. This scenario is described by Tvergaard (1985) and Riedel (1987).

However, the results support the suggestion of the existence of a transition zone (in stress), where none of the above failure mechanism predominates, and where the combined ductile–brittle mechanism should be introduced instead. In this zone, the failure results from both the large creep strains and the material deterioration due to the nucleation of voids.

In order to describe the above features within a phenomenological approach, different models of damage have been introduced.

2.2.1. Viscoplastic damage model for brittle and combined ductile–brittle failure mechanisms

If we consider brittle fracture at low stress without geometrical effect, we can assume a time dependent damage evolution. In this case, for a constant applied load, creep damage increases with time and the geometrical effect is not necessary to describe the tertiary creep period. However, we can introduce nonlinear geometrical effects in order to display a transition zone, where the combined ductile–brittle failure mechanism results from both material deterioration on grain boundaries and reduction of the cross-sectional area due to large creep strains within the grain. Indeed, beyond strains of a few percent, the true stress significantly increases rather than remaining constant. This increase may induce a creep strain enlargement. With this approach, we may obtain a viscoplastic damage model in nonlinear geometry, where inelastic and damage processes are time dependent.

The relation (17) specifies the evolution of the damage variable X by means of the damage dissipation potential φ_X^*. It has been shown experimentally that there exists a finite region in space stress (strain) within which materials exhibit elastic–viscoplastic behavior without any development of damage (Holcomb and Costin, 1986). Therefore, just like the viscoplastic potential, we assume the existence of a time dependent yield function of damage and a damage potential in the space of the thermodynamics conjugate forces. Thus, one of the simplest convex function for the damage dissipation potential may be given as for viscoplastic flow:

$$\varphi_X^* = \frac{1}{n_x+1}\langle f_X(Y)\rangle_+^{n_x+1} = \frac{1}{n_x+1}\langle -Y-Z_0\rangle_+^{n_x+1} \tag{23}$$

with $f_X(Y) = -Y - Z_0 = \frac{1}{2}\mathrm{tr}(\sigma C e^{-1}\sigma) - Z(X) - Z_0$.

The expression of the damage evolution law is given by Eqs. (11) and (17):

$$\dot{X} = -\frac{\partial\varphi_X^*}{\partial Y} = \left\langle \frac{1}{2}\mathrm{tr}(\sigma C e^{-1}\sigma) - Z(X) - Z_0 \right\rangle_+^{n_x} \tag{24}$$

$Z(X)$ is given by Eq. (10). $Z(X)$ may be chosen as follows:

$$Z(X) = \rho\frac{\partial\psi_X}{\partial X} = q(1-\exp(-cX)), \tag{25}$$

where the material parameters n_x, q and c control the damage evolution. $Z_0 \geqslant 0$ denotes the initial damage limit.

2.2.2. Viscoplastic viscodamage model for ductile failure mechanism

If we consider that the tertiary creep stage arises from ductile phenomena at high stress, a viscoplastic model in nonlinear geometry can describe this tertiary creep period. However, cavities subsequently grow further by the creep deformation. Therefore, we introduce damage effects in the model, in order to display this rapid evolution of damage at the end of the creep life in addition to the influence of nonlinear geometrical effects of changes in geometry on the strain rate. Unlike the above viscoplastic damage model, where the creep damage increased with time, and where the geometrical effect was not necessary to have damage evolution, the viscoplastic viscodamage model requires this geometrical effect. With this approach, damage evolution is not directly linked with time. It is the coupling between viscoplasticity and geometrical nonlinearities which allows the increase of stress under constant applied load and consequently the increase in damage. We obtain a viscoplastic viscodamage model in the nonlinear geometry where viscoplastic process is always time dependent. The basic idea in the formulation of this model is the following: The damage directly affects the material elastic stiffness. It is the coupling between the model and geometrical nonlinearities which enables strain softening to occur.

The relation (17) specifies the evolution of the damage variable X by means of the damage potential φ_X^*. In the viscoplastic damage model, an important distinction from the viscoplastic viscodamage model stems from the fact that the current stress states can be outside the yield surface of damage, and that the yield function may have a value larger than zero. Therefore, the consistency conditions are not applicable. When the external loading remains constant, the stresses return to the yield surface as a function of time. Now, the damage potential of dissipation is chosen as the indicator function of the damage convex defined by the yield function:

$$f_X(Y) = -Y - Z_0 = \frac{1}{2}\mathrm{tr}(\sigma C e^{-1}\sigma) - Z(X) - Z_0 \leqslant 0, \tag{26}$$

where $Z_0 \geqslant 0$ is the initial damage threshold.

Damage occurs only when the state of stress reaches the actual yield function. This corresponds to the satisfaction of the yield criterion $f_X = 0$. Damage continues to grow, if the yield is continuously satisfied, i.e. if $\dot{f}_X = 0$. The expression of the damage evolution law is given by Eqs. (11) and (17):

$$\dot{X} = -\lambda_X \frac{\partial f_X}{\partial Y} = \lambda_X. \tag{27}$$

The expression of the damage multiplier $\lambda_X \geqslant 0$ is deduced from the consistency conditions $f_X = 0$ and $\dot{f}_X = 0$.

$Z(X)$ is given by Eq. (10). $Z(X)$ may be chosen as follows:

$$Z(X) = \rho \frac{\partial \psi_X}{\partial X} = \frac{\ln(1+X)}{A}, \tag{28}$$

the material parameter A controls the damage evolution.

2.3. Viscoplastic (visco)damage models in nonlinear geometry

Nonlinear geometrical effects defined above, are described by writing in nonlinear geometry, the models previously developed in small perturbations. We may consider an initial configuration Ω_0. Loads F_{d_0} are applied to a part $\partial_2\Omega_0$ on its boundary, and displacements u_{d_0} on the part $\partial_1\Omega_0$. Body forces density f_{d_0} is also applied. M_0 is a point on Ω_0 which we find at M at the instant t Fig. 1. M is defined by $M = M_0 + u(M_0, t)$, where $u(M_0, t)$ is the displacement field.

We may define the various kinematic and static variables used:

F, the gradient tensor

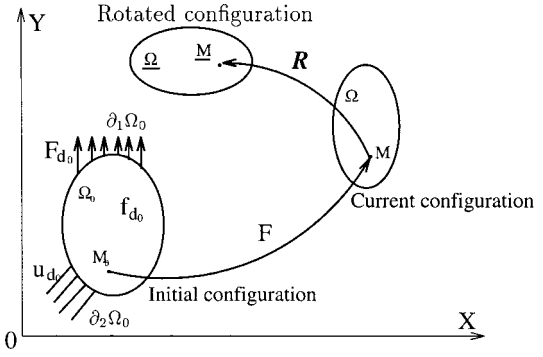

Fig. 1. Corotational model and boundary conditions.

$$F = I + \frac{\mathrm{d}u(M_0, t)}{\mathrm{d}M_0},$$

L, the velocity gradient tensor

$$L = \dot{F}F^{-1},$$

D, the strain rate tensor

$$D = \tfrac{1}{2}(L + L^{\mathrm{T}}),$$

W, the rotation rate tensor

$$W = \tfrac{1}{2}(L - L^{\mathrm{T}}),$$

τ, the Kirchhoff stress tensor

$$\tau = J\sigma,\ J = \det F.$$

P, the first Piola–Kirchhoff stress tensor

$$P = J\sigma F^{-\mathrm{T}}.$$

Generally, the variables used to describe the constitutive laws in nonlinear geometry are not objective. To be objective, we consider the following kinematic model of Ladevèze (1981). It introduces for all points of the domain a local rotation $\boldsymbol{R}$, defining the corotational configuration $\underline{\Omega}$. This rotation locally transforms the configuration of Ω into a rotated configuration $\underline{\Omega}$ Fig. 1. $\mathbf{R}$ is associated to the rotation rate W, and defined by the differential equation and the conditions:

$$\begin{cases} \dot{\mathbf{R}}^{\mathrm{T}}\mathbf{R} = W = \tfrac{1}{2}(L - L^{\mathrm{T}}), \\ \mathbf{R}_{|t=0} = I, \quad \mathbf{R}\mathbf{R}^{\mathrm{T}} = I. \end{cases} \tag{29}$$

With this rotation, we obtain the strain rate and the stress tensor in the corotational configuration:

$$\begin{cases} \underline{\tau} = \mathbf{R}\tau\mathbf{R}^{\mathrm{T}} \\ \underline{D} = \mathbf{R}D\mathbf{R}^{\mathrm{T}} \end{cases} \tag{30}$$

the symbol $\underline{x}$ means that the variable is expressed in the corotational configuration.

Furthermore, $\dot{\underline{\tau}}$ the Kirchhoff stress in the rotated configuration takes the following form:

$$\dot{\underline{\tau}} = \mathbf{R}\tau^{\mathrm{J}}\mathbf{R}^{\mathrm{T}} \tag{31}$$

τ^{J} denotes the Jaumann rate of the Kirchhoff stress and $\dot{\underline{\tau}} = \underline{\tau}^{\mathrm{J}}$; Eq. (31) defined as an objective stress rate.

We obtain the viscoplastic (visco) damage models in nonlinear geometry by writing the corotational configuration of the geometrical model between $\dot{\underline{\tau}}$ and $\underline{D}$, the models developed above in small perturbations. Then, material behavior laws are objective constitutive laws (Rougée, 1991). The extension of the models in nonlinear geometry is outlined in the text below, which shows the constitutive equations as follows (see also Table 1):

$\rho\psi(\underline{\varepsilon}_e, X, p) = \rho\psi_e(\underline{\varepsilon}_e, X) + \rho\psi_{vp}(p) + \rho\psi_X(X)$ (the free energy),

$$\rho\psi_e(\underline{\varepsilon}_e, X) = \frac{1}{2}\frac{\mathrm{tr}(\underline{\varepsilon}_e C_e \underline{\varepsilon}_e)}{1+X} \quad \text{with} \quad \underline{\varepsilon} = \int_0^T \underline{D}\,\mathrm{d}t$$

$$\text{with } \underline{D} = \underline{D}_e + \underline{D}_{vp} \quad \text{and} \quad \underline{\varepsilon}_e = \int_0^T \underline{D}_e\,\mathrm{d}t, \quad \underline{\varepsilon}_{vp} = \int_0^T \underline{D}_{vp}\,\mathrm{d}t,$$

where $\underline{D}_e$ is the rotated elastic strain rate and $\underline{D}_{vp}$ is the rotated viscoplastic strain rate.
The constitutive laws:

$$\underline{\tau} = \rho\frac{\partial\psi_e}{\partial\underline{\varepsilon}_e} = \frac{C_e}{1+X}\underline{\varepsilon}_e, \qquad R = \rho\frac{\partial\psi_{vp}}{\partial p} = Q(1-\exp(-bp)),$$

$$Y = \rho\frac{\partial\psi_e}{\partial X} + \rho\frac{\partial\psi_X}{\partial X} = -\frac{1}{2}\mathrm{tr}(\underline{\tau}C_e^{-1}\underline{\tau}) + Z(X), \quad Z(X) = \rho\frac{\partial\psi_X}{\partial X}.$$

$$\Phi = \mathrm{tr}(\underline{\tau}\underline{D}_{vp}) - Y\dot{X} - R\dot{p} \geqslant 0 \quad \text{(the intrinsic dissipation)},$$

$$\varphi^*(\underline{\tau}, R, Y) = \varphi^*_{vp}(\underline{\tau}, R) + \varphi^*_X(Y) \quad \text{(the dissipation potential)}.$$

The complementary evolution laws:

$$\underline{D}_{vp} = \frac{\partial\varphi^*_{vp}(\underline{\tau}, R)}{\partial\underline{\tau}}, \quad \dot{p} = -\frac{\partial\varphi^*_{vp}(\underline{\tau}, R)}{\partial p}, \quad \dot{X} = -\frac{\partial\varphi^*_X(Y)}{\partial Y}.$$

Table 1
Constitutive equations in nonlinear geometry

Viscoplastic damage model	Viscoplastic viscodamage model
$\varphi^*_{vp} = \frac{K}{n+1}\left\langle\frac{\tau_{eq}-R(p)-R_0}{K}\right\rangle_+^{n+1}$	$\varphi^*_{vp} = \frac{K}{n+1}\left\langle\frac{\tau_{eq}-R(p)-R_0}{K}\right\rangle_+^{n+1}$
with $\tau_{eq} = \sqrt{\frac{3}{2}\mathrm{tr}(\underline{\tau}_D\underline{\tau}_D)}$	with $\tau_{eq} = \sqrt{\frac{3}{2}\mathrm{tr}(\underline{\tau}_D\underline{\tau}_D)}$
and $\underline{\tau}_D$ the deviatoric part of $\underline{\tau}$,	and $\underline{\tau}_D$ the deviatoric part of $\underline{\tau}$,
$\varphi^*_X = \frac{1}{n_x+1}\left\langle\frac{1}{2}\mathrm{tr}(\underline{\tau}C_e^{-1}\underline{\tau}) - Z(X) - Z_0\right\rangle_+^{n_x+1}$,	$f_X(Y) = \frac{1}{2}\mathrm{tr}(\underline{\tau}C_e^{-1}\underline{\tau}) - Z(X) - Z_0 \leqslant 0$,
$\underline{D}_{vp} = \frac{3}{2}\frac{\underline{\tau}_D}{\tau_{eq}}\dot{p}$,	$\underline{D}_{vp} = \frac{3}{2}\frac{\underline{\tau}_D}{\tau_{eq}}\dot{p}$,
$\dot{p} = \left\langle\frac{\tau_{eq}-R(p)-R_0}{K}\right\rangle_+^n$,	$\dot{p} = \left\langle\frac{\tau_{eq}-R(p)-R_0}{K}\right\rangle_+^n$,
$\dot{X} = \left\langle\frac{1}{2}\mathrm{tr}(\underline{\tau}C_e^{-1}\underline{\tau}) - Z(X) - Z_0\right\rangle_+^{n_x}$,	$\dot{X} = -\lambda_X\frac{\partial f_X(Y)}{\partial X} = \lambda_X$,
$Z(X) = q(1-\exp(-cX))$.	$Z(X) = \frac{\ln(1+X)}{A}$.

3. Numerical treatment by the large time increment method

Numerical simulation of creep behavior with classic software leads to small and therefore numerous loading time increments, which in turn leads to a large number of global resolutions. Unlike the classical incremental methods of the Newton–Raphson type, which break up the loading interval into small increments, the LATIN method (Boisse et al., 1990) consists of designing an iterative scheme which, at each iteration, gives an approximation to the solution for large loading increment (large time increment for creep behavior). The LATIN method enables us to describe large creep life in a few increments, in order to reduce the calculation cost. With this method, we can swiftly reach the tertiary creep period, which involves most nonlinearities in order to obtain a creep life assessment.

3.1. Iterative scheme

The iterative scheme of this method provides at each iteration a new estimation of the solution on $\Omega_0 \times [0,T]$, for large time increment, and not for small increment by small increment and it does so until convergence occurs. As for steady state problems, each iteration progresses from an admissible estimation $S_n = [\dot{F}_n, \dot{P}_n] \in A_d$ to another better estimation $S_{n+1} = [\dot{F}_{n+1}, \dot{P}_{n+1}] \in A_d$ verifying the kinematic and the static admissibilities on $\Omega_0 \times [0,T]$. Each iteration is split into two steps: Firstly, a nonlinear and local step (in space), which leads to a calculated intermediate estimation $\hat{S}_n = [\hat{\dot{F}}_n, \hat{\dot{P}}_n] \in \Gamma$, verifying the behavior laws. Secondly, a global (in space) and linear step, which gives $S_{n+1} = [\dot{F}_{n+1}, \dot{P}_{n+1}] \in A_d$. The global iterative process ceases when the error $\|\hat{S}_n - S_{n+1}\|$ is sufficiently low.

Before beginning this presentation, we will present the mechanical problem in nonlinear geometry in a form compatible with the LATIN method initially developed in small perturbations (Bussy et al., 1990).

Problem: find $S_e = A_d \cap \Gamma$

$$S_n \in A_d \Longleftrightarrow \begin{cases} \exists u_n(M_0,t)/u(M_0,0) = 0 \quad \text{and} \quad \dot{u}(M_0,0) = 0, \\ \dot{u}_n(M_0,t)\,|_{\partial_1\Omega_0} = \dot{u}_d \quad \text{and} \quad \dot{F}_n = \frac{\partial \dot{u}_n}{\partial M_0}, \\ \forall t \in [0,T],\ \forall u^*/u^*\,|_{\partial_1\Omega_0} = 0 \quad \text{and} \quad u^*(M_0,0) = 0, \\ \int_{\Omega_0} \operatorname{tr}(\dot{P}_n^{\mathrm{T}} F^*)\,\mathrm{d}\Omega_0 = \int_{\partial_2\Omega_0} \dot{F}_{\mathrm{d}_0}\ u^*\,\mathrm{d}S_0 + \int_{\Omega_0} \dot{f}_{d_0}\ u^*\,\mathrm{d}\Omega_0. \end{cases} \tag{32}$$

$$\hat{S}_n \in \Gamma \Longleftrightarrow \hat{\dot{F}}_{n_t} = \mathscr{A}(\hat{P}_{n_\eta}, \eta \leqslant t), \tag{33}$$

where $\mathscr{A}$ is an operator representing the behavior law. $\mathscr{A}$ presents the material and the geometrical nonlinearities. The algorithm is in the form of a series of iterations on large time increment in which each iteration is in two steps between the two sets A_d and Γ.

In practice, the global step is transformed in order to write $S_{n+1} \in A_d$ in the following form:

$$S_{n+1} = S_n + \Delta S_{n+1} \tag{34}$$

or $[\dot{F}_{n+1}, \dot{P}_{n+1}] = [\dot{F}_n, \dot{P}_n] + [\Delta\dot{F}_{n+1}, \Delta\dot{P}_{n+1}]$

$$\text{or } S_{n+1} = S_0 + \sum_{i=0}^{n+1} \Delta S_i, \tag{35}$$

where S_0 is an elastic initialization and n the number of iterations. ΔS_{n+1} must be kinematically and statically admissible at 0.

Local step: knowing $S_n = [\dot{F}_n, \dot{P}_n] \in A_d$, construct $\hat{S}_{n+1} = [\hat{\dot{F}}_{n+1}, \hat{\dot{P}}_{n+1}] \in \Gamma$ verifying on $[0, T]$:

$$\hat{\dot{F}}_{n+1_t} = \mathscr{A}(\hat{P}_{n+1_\eta}, \eta \leqslant t) \text{ in } \Omega_0 \tag{36}$$

$$\text{with } \hat{\dot{F}}_{n+1} = \dot{F}_n \text{ in } \Omega_0. \tag{37}$$

Global step: from $\hat{S}_{n+1} = [\hat{\dot{F}}_{n+1}, \hat{\dot{P}}_{n+1}] \in \Gamma$, find $\Delta S_{n+1} = [\Delta\dot{F}_{n+1}, \Delta\dot{P}_{n+1}] \in A_d$ verifying on $[0, T]$:

$$\begin{cases} \exists\, \Delta\dot{u}_{n+1}/\Delta\dot{F}_{n+1} = \frac{\partial \Delta\dot{u}_{n+1}}{\partial M_0} \quad \text{and} \quad \Delta\dot{u}_{n+1}\,|_{\partial_1\Omega_0} = 0, \\ \forall\, u^*/u^*\,|_{\partial_1\Omega_0} = 0 \quad \text{and} \quad u^*(M_0, 0) = 0, \\ \int_{\Omega_0}\int_0^T \operatorname{tr}\left[F^{*T} C_e\, \Delta\dot{F}_{n+1}\right] \mathrm{d}t\, \mathrm{d}\Omega_0 = \int_{\Omega_0}\int_0^T \operatorname{tr}\left[F^{*T}(\dot{P}_n - \hat{\dot{P}}_{n+1})\right] \mathrm{d}t\, \mathrm{d}\Omega_0. \end{cases} \tag{38}$$

The act of writing the above global problem (38) in this variational form and in this kinematic approach for the finite element resolution, arises from the choice of the search direction (37) between the global and the local steps and the search direction:

$$\hat{\dot{P}}_{n+1} - \dot{P}_{n+1} = C_e(\hat{\dot{F}}_{n+1} - \dot{F}_{n+1}) \tag{39}$$

between the local and the global steps.

Search directions defined by Eqs. (37) and (39) characterize the LATIN method version. With these choices, the iterative algorithm is like a modified Newton method.

3.2. Representation of the unknowns

There are no special difficulties about the local step. The question is to solve a nonlinear problem for the interval $[0, T]$ at any integration point M_0. The greatest difficulty is to solve the global problem (38), which is parameterized by time on the interval $[0, T]$. In order not to solve the global problem for each time, this problem is divided into two problems. A first space problem which depends only on the space variable M_0, and a second time problem which depends only on time. To obtain at each iteration a new estimation solution over the large time increment, the idea is to represent at each iteration the unknowns in the following form:

$$\begin{aligned} \Delta\dot{u}_{n+1} &= \dot{u}_{n+1}(t, M_0) - \dot{u}_n(t, M_0) = \sum_{i=1}^{p} g_i(t)\ w_i(M_0), \\ \Delta\dot{F}_{n+1} &= \dot{F}_{n+1}(t, M_0) - \dot{F}_n(t, M_0) = \sum_{i=1}^{p} g_i(t)\ \alpha_i(M_0), \\ \Delta\dot{P}_{n+1} &= \dot{P}_{n+1}(t, M_0) - \dot{P}_n(t, M_0) = \sum_{i=1}^{p} h_i(t)\ \beta_i(M_0), \end{aligned} \tag{40}$$

where $g_i(t)$ and $h_i(t)$ defined on $[0, T]$ are scalar time function constant for each integration time step of the behavior law. p is the number of time functions at each iteration. The fields $w_i(M_0)$, $\alpha_i(M_0)$ and $\beta_i(M_0)$ depend only on the space variable M_0. With $\alpha_i(M_0) = \frac{\mathrm{d}w_i}{\mathrm{d}M_0}$ and $\alpha_i(M_0)$ KA at 0 and $\beta_i(M_0)$ SA at 0.

For more details concerning the numerical treatment by the LATIN method, see Bussy et al. (1990) and Bellenger (1998b). To sum up, a scheme of the algorithm is presented in Fig. 2, in comparison with classical incremental method Fig. 3, where K is the stiffness matrix, $\mathrm{d}U_i$ is the nodal vector of space variables $\mathrm{d}u_i$ and F_i the second member. The space variable $\alpha_i(M_0)$ is equal to $B\,\mathrm{d}U_i$, where B is the derivative matrix of the basis functions.

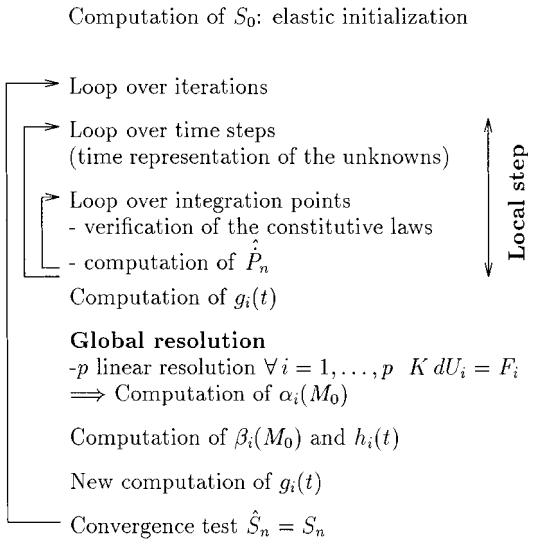

Fig. 2. LATIN method algorithm.

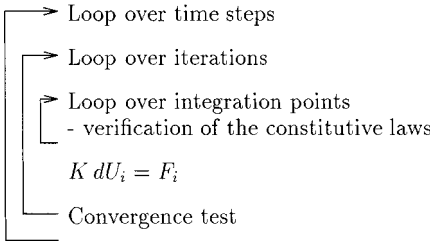

Fig. 3. Classic incremental method algorithm.

3.3. Algorithmic aspects

From the computational point of view, the above constitutive equations (see the constitutive equations in Section 2.3 and Table 1) must be integrated during the local step. In displacement-based finite element formulations, stress updates take place at the Gauss points for a prescribed nodal displacement. We start from time t with the known converged state: $[\underline{\varepsilon}_t, \underline{\varepsilon}_{\mathrm{vp}_t}, \underline{\tau}_t, p_t, X_t]$ to calculate the corresponding value at time $t + \Delta t$: $[\underline{\varepsilon}_{t+\Delta t}, \underline{\varepsilon}_{\mathrm{vp}_{t+\Delta t}}, \underline{\tau}_{t+\Delta t}, p_{t+\Delta t}, X_{t+\Delta t}]$ with a prescribed incremental nodal displacement.

$$\hat{F}_{t+\Delta t} = \hat{F}_t + \Delta\hat{F}. \tag{41}$$

Therefore, from the definition of the strain rate tensor D,

$$\Delta\varepsilon = \frac{1}{2}\left[\Delta\hat{F}\,\hat{F}_{t+\Delta t}^{-1} + (\Delta\hat{F}\,\hat{F}_{t+\Delta t}^{-1})^{\mathrm{T}}\right]. \tag{42}$$

A numerical resolution of the differential equation (29) allows to obtain $\mathbf{R}_{t+\Delta t}$ and

$$\Delta\underline{\varepsilon} = \mathbf{R}_{t+\Delta t}\,\Delta\varepsilon\,\mathbf{R}_{t+\Delta t}^{\mathrm{T}}. \tag{43}$$

The key feature of stress updates is characterized by estimating the incremental viscoplastic strain $\Delta\underline{\varepsilon}_{\mathrm{vp}}$ and the incremental damage ΔX. We can perform an elastic predictor, assuming that the viscoplastic and

the damage variables remain frozen. The trial elastic stress $\underline{\tau}_{\mathrm{tr}}$ can be computed by the constitutive law in Section 2.3.

$$\begin{cases} \underline{\tau}_{\mathrm{tr}} = \underline{\tau}_t + \frac{C_{\mathrm{e}}}{1+X_t}\,\Delta\underline{\varepsilon}, \\ p_{t+\Delta t} = p_t, \\ X_{t+\Delta t} = X_t. \end{cases} \tag{44}$$

3.3.1. Viscoplastic damage model

If $\underline{\tau}_{\mathrm{tr}}$ lies outside the viscoplastic domain f_{vp} and the damage domain f_X, a viscoplastic-damage corrector step is then carried out by using for example a simple Euler forward integration scheme (explicit method). Therefore (see Table 1),

$$\begin{cases} p_{t+\Delta t} = p_t + \Delta p = p_t + \Delta t\,\dot{p}_t \quad \text{with} \quad \dot{p}_t = \left\langle \frac{(\tau_{\mathrm{eq}_t}) - R(p_t) - R_0}{K} \right\rangle_+^n \\ X_{t+\Delta t} = X_t + \Delta X = X_t + \Delta t\,\dot{X}_t \quad \text{with} \quad \dot{X}_t = \left\langle \frac{1}{2}\,\mathrm{tr}\,(\underline{\tau}_t\, C_{\mathrm{e}}^{-1}\,\underline{\tau}_t] - Z(X_t) - Z_0 \right\rangle_+^{n_x}. \end{cases} \tag{45}$$

Damage and inelastic phenomena evolutions lead to the stress tensor at $t+\Delta t$ as:

$$\underline{\tau}_{t+\Delta t} = \frac{C_{\mathrm{e}}}{1+X_{t+\Delta t}}\left[\underline{\varepsilon}_{t+\Delta t} - \underline{\varepsilon}_{\mathrm{vp}_{t+\Delta t}}\right] = \frac{C_{\mathrm{e}}}{1+X_{t+\Delta t}}\left[\underline{\varepsilon}_{t+\Delta t} - \underline{\varepsilon}_{\mathrm{vp}_t} - \Delta\underline{\varepsilon}_{\mathrm{vp}}\right]. \tag{46}$$

Substitution of $\underline{\varepsilon}_{\mathrm{vp}_t} = -C_{\mathrm{e}}^{-1}\,\underline{\tau}_t(1+X_t) + \underline{\varepsilon}_t$ (see Table 1) into Eq. (46) yields

$$\underline{\tau}_{t+\Delta t} = \frac{C_{\mathrm{e}}}{1+X_{t+\Delta t}}\left[\Delta\underline{\varepsilon} - \Delta\underline{\varepsilon}_{\mathrm{vp}}\right] + \underline{\tau}_t\,\frac{1+X_t}{1+X_{t+\Delta t}} \tag{47}$$

in which (see Table 2)

$$\Delta\underline{\varepsilon}_{\mathrm{vp}} = \frac{3}{2}\,\frac{\underline{\tau}_{D_t}}{\underline{\tau}_{\mathrm{eq}_t}}\,\Delta p. \tag{48}$$

Now $\hat{P}_{t+\Delta t}$ becomes

$$\hat{P}_{t+\Delta t} = \mathbf{R}_{t+\Delta t}^T\,\underline{\tau}_{t+\Delta t}\,\mathbf{R}_{t+\Delta t}\,\hat{F}_{t+\Delta t}^{-T}. \tag{49}$$

Table 2
Summary of material parameters for IN 100 at 1000°C

Parameters	IN 100 (1000°C)
E (MPa)	147 000
v	0.3
n	7.5
K	450
R_0	0
Q	95
b	6000
n_x	4.5
q	0.5
c	0.038
Z_0	0

3.3.2. Viscoplastic viscodamage model

The trial elastic stress $\underline{\tau}_{\mathrm{tr}}$ is given by Eq. (44). If stress lies outside the viscoplastic domain f_{vp}, a viscoplastic corrector step is then carried out as in the above model. If the stress lies outside the damage domain f_X, a viscodamage corrector is carried out using the algorithm stated by Ortiz and Simo (1986).

In this consistency approach (for damage), at each iteration, the stress is relaxed in a step-by-step process. For each iteration (j), the damage multiplier $\lambda_X = \dot{X}$ [see Table 1] is determined by the discretized consistency condition of the damage yield surface. For each iteration, f_X is linearized around the current values of the state variables as

$$f_{X_{t+\Delta t}}^{(j+1)} \simeq f_{X_{t+\Delta t}}^{(j)} + \left(\frac{\partial f_X^{(j)}}{\partial \underline{\tau}}\right)_{t+\Delta t} \Delta \underline{\tau}_X^{(j+1)} + \left(\frac{\partial f_X^{(j)}}{\partial X}\right)_{t+\Delta t} \Delta X^{(j+1)}. \tag{50}$$

The damage multiplier is determined by requiring $f_{X_{t+\Delta t}}^{(j+1)} \simeq 0$. Differentiating the constitutive law of $\underline{\tau}$ (see the constitutive equations in Section 2.3), we may obtain damage stress variation $\Delta \underline{\tau}_X^{(j+1)}$ in the following form:

$$\Delta \underline{\tau}_X^{(j+1)} = -\frac{C_{\mathrm{e}}}{(1 + X_{t+\Delta t}^{(j)})^2}\, \underline{\varepsilon}_{\mathrm{e}}\, \Delta X^{(j+1)}. \tag{51}$$

Substitution of the constitutive law of $\underline{\tau}$ into Eq. (51) gives

$$\Delta \underline{\tau}_X^{(j+1)} = -\frac{\underline{\tau}_{t+\Delta t}^{(j)}}{1 + X_{t+\Delta t}^{(j)}}\, \Delta X^{(j+1)}. \tag{52}$$

Substitution of Eq. (52) into Eq. (50) gives

$$\Delta X^{(j+1)} = \frac{f_{X_{t+\Delta t}}^{(j)}}{\frac{\mathrm{tr}(\underline{\tau}_{t+\Delta t}^{(j)} C_{\mathrm{e}}^{-1} \underline{\tau}_{t+\Delta t}^{(j)})}{1+X_{t+\Delta t}^{(j)}} + Z'(X_{t+\Delta t}^{(j)})} \tag{53}$$

and

$$X_{t+\Delta t}^{(j+1)} = X_t + \sum_{i=1}^{j+1} \Delta X^{(i)}, \tag{54}$$

$\underline{\tau}_{t+\Delta t}^{(j+1)}$ is given by Eq. (47). The iterative process ceases when $f_{X_{t+\Delta t}}^{(j+1)} \simeq 0$.

4. Numerical examples

The creep constitutive models in nonlinear geometry, presented above, have been implemented in our finite element code OPTIFIA using the LATIN method. The elements used are isoparametric six-node triangles with three Gauss points.

Firstly, the viscoplastic damage model has been used for uniaxial tensile creep behavior, in order to display the modeling and the numerical resolution capabilities. After that, finite element computational results have been obtained for the creep analysis of notched plates and double edge cracked plates, where stress gradients exist. It has been shown how this model has the capability to describe the lifetimes and the patterns of damage evolution. Secondly, the viscoplastic viscodamage model has been used for an L-shaped structure in order to show the capability and the characteristics of this approach to describe the development of damage in creeping components. Finally, we have used the models on the same structure, in order to display different modes of damage development and their dependences on the level of stress.

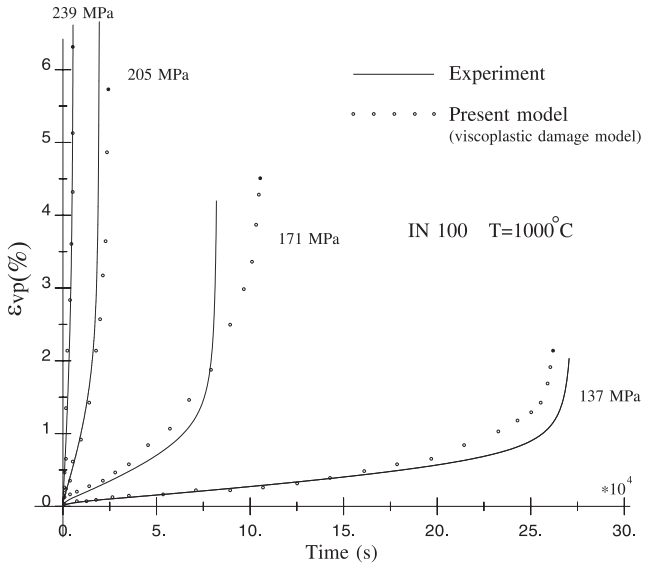

Fig. 4. Comparison of the experimentally obtained strain-time with predicted IN 100 at 1000°C.

4.1. Example 1: uniaxial creep behavior

To test the viscoplastic damage model, we must compare its predictions against uniaxial creep results concerning IN 100 at 1000°C (Lemaitre and Chaboche, 1985). In this example, the stress state is uniform, the level of damage is also uniform. The values of the parameters for this material are given in Table 2. Fig. 4 shows the uniaxial creep curves of IN 100 under different levels of applied load (constant applied load). The prediction of the uniaxial tensile creep behavior by the present model and experimental results concord well.

In addition to the influence of damage on the strain rate, the nonlinear effects of changes in geometry may also significantly contribute to tertiary creep. In the constant load tensile test, this amounts to the uniform thinning of the area cross-section at increasing longitudinal strain. For metals with negligible damage rates, it is this mechanism, which is primarily responsible for tertiary creep and subsequent rupture. The viscoplastic damage model used in this example can describe this nonlinear geometrical phenomenon. In Fig. 5, the behavior of the model is compared with the model in small perturbations (constant stress test) as well as the behavior of the model without damage for IN 100 at 137 MPa. In this case, it can be seen that the interaction between the geometrical effect and damage is not important. For this material, the geometrical effect is far less significant than damage. Neglecting the geometrical effect results in an error of about 4% in fracture time while neglecting damage results in an error of about 300% in fracture time. In this case, we have described a brittle rupture phenomenon. However, for a material with a more important primary creep period (Fig. 6(A), Curves 1 and 2), it can be seen that the interaction between the geometrical effect and damage produces a more pronounced tertiary creep period than that obtained by neglecting either one of the effects. Neglecting the geometrical effect results in an error of about 16% in fracture time (Fig. 6(A), Curve 2). Therefore, tertiary creep arises more from interaction between damage and geometrical nonlinearities, these results emphasizes a combined ductile–brittle failure mechanism. This more important coupling can be seen in Fig. 6(B). For Curve 2, the stress continuously grows with time during loading when for Curve a, the increase of stress takes place sufficiently early in the lifetime of the specimen to enable the rupture life to be predicted in small perturbations.

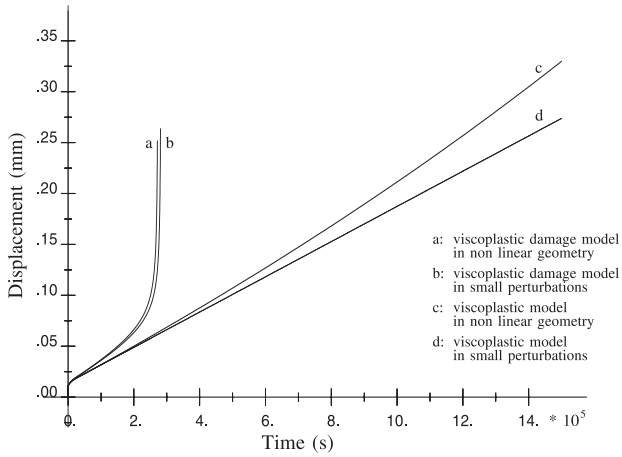

Fig. 5. Effect of damage and geometrical nonlinearities for IN 100 at 137 MPa.

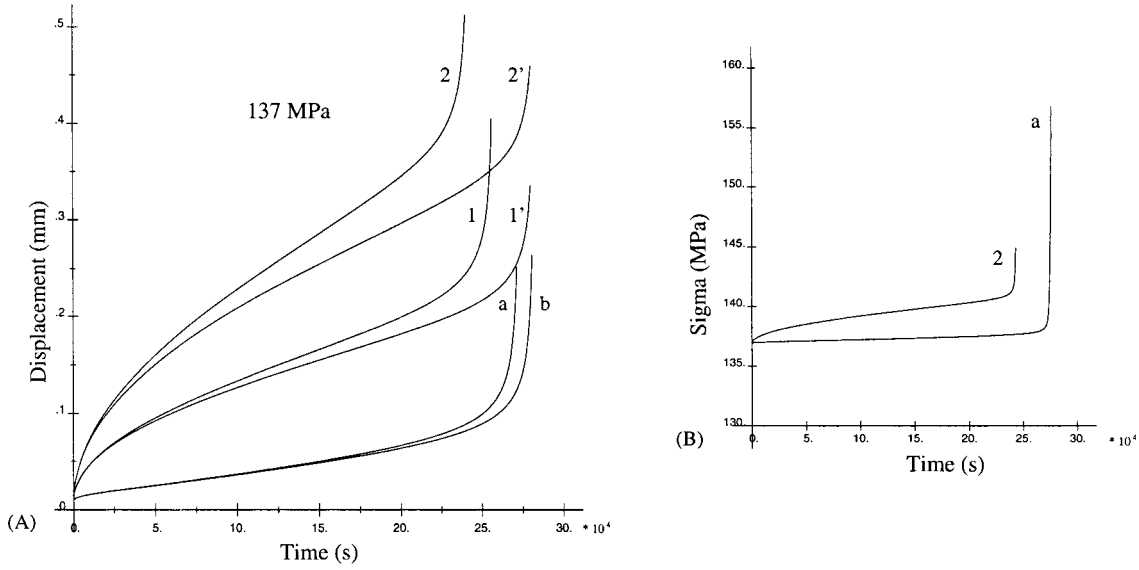

Fig. 6. (A) Effect of geometrical nonlinearities; (B) Evolution of σ. Curves b, 1′ and 2′ are in small perturbations. Curves a, b and 2 are in nonlinear geometry. For curves a and b see Fig. 5.

4.1.1. Numerical analysis

To measure the performance of the LATIN method considered in this study, for results concerning the above example, we may compute a reference solution with a large number of increments until results do not change. To assess the performance of the LATIN method, two errors have been defined for IN 100 at 137 MPa. er_2 is an error in displacement between the reference solution and the calculations for a loading of 20 000 seconds, er_1 is an error in time between the reference solution and the calculations for a displacement of 0.2%. All runs were performed on an HP 9000 C160 workstation.

First of all (Table 3), a decrease in the number of increments (with 40 time steps per load time increment) allows us to divide the iterations by 5.6 keeping er_1 and er_2 small. In the case of four load time increments,

Table 3
Numerical analysis of IN 100 results

	Reference				
Number of LATIN increments	33	33	19	9	4
Number of time steps	2640	1320	760	360	160
Number of LATIN iterations	107	94	65	37	19
CPU time (s)	508	240	135	72	30
er_1		0.036%	0.09%	0.22%	0.71%
er_2		0.008%	0.036%	0.062%	0.3%

Table 4
Numerical analysis of IN 100 results

Number of LATIN increments	2	2	1
Number of time steps	140	400	200
Number of LATIN iterations	4	5	2
CPU time (s)	17	59	27
er_1	2%	0.19%	0.35%
er_2	1.8 %	0.03 %	

the CPU time varied from 508 to 30 s (Table 3). It is possible to improve this by describing the three creep periods with two increments. If we emphasize the speed, only 17 s are required (Table 4). If we emphasize the accuracy, 59 s are required for $er_1 = 0.19\%$ and $er_2 = 0.03\%$ (Table 4). However, the LATIN method enables this problem to be simulated with only one increment and two iterations with a good value for er_1. Therefore, $2 \times p$ global resolutions have been necessary ($p = 10$), p is defined in Eq. (40). With classic incremental method, at least 200 global resolutions would be necessary to obtain the same time discretization (200 time steps).

4.2. Example 2: creep damage analysis of edge cracked plates

A better understanding of the development of damage in creeping components is essential in design as well as in the estimation of creep life. The information that is needed for life predictions is a reliable model for the accumulation of creep damage. It is then important to describe the possible localizations of this damage in regions of strain concentrations, such as notches and cracks. Therefore, finite element computational results have been obtained for edge cracked plates. The geometry, mesh and boundary conditions are shown in Fig. 7. We will take one half of the edge cracked plates. The values of the parameters used in the viscoplastic damage model are given in Table 2.

The creep strain distribution in double edge cracked plate is plotted in Fig. 8(d). For this geometry, the creep strains concentrate along inclined planes with respect to the initial crack plane. The resulting damage contours are plotted in Fig. 8(b). It is clear that a damage zone is propagating along an inclined plane with respect to the initial crack plane. It should be noted that as the creep strains increase, the initial sharp crack tip becomes more and more blunted. Because of this effect, the specimen develops a notch-like behavior and the damaged zone begins to concentrate in later stage in the symmetry plane of the crack. The macrocracks then develop two branches. This tendency can be seen in Fig. 8(b). A plate containing a central slit has been selected too. The distribution of accumulated creep strains is shown in Fig. 8(c). Fig. 8(a) shows the contours of damage distribution. A damage zone is propagating along two inclined zones with respect to the initial crack plane. Fig. 9 shows how a central slit reduces the creep rupture lifetime with regard to a

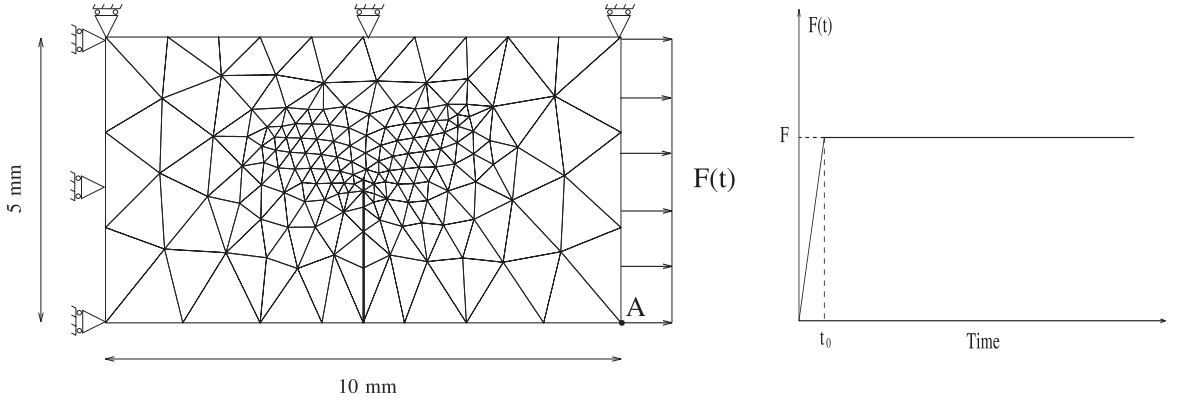

Fig. 7. Geometry, mesh and boundary conditions of edge cracked plate ($F = 100$ MPa).

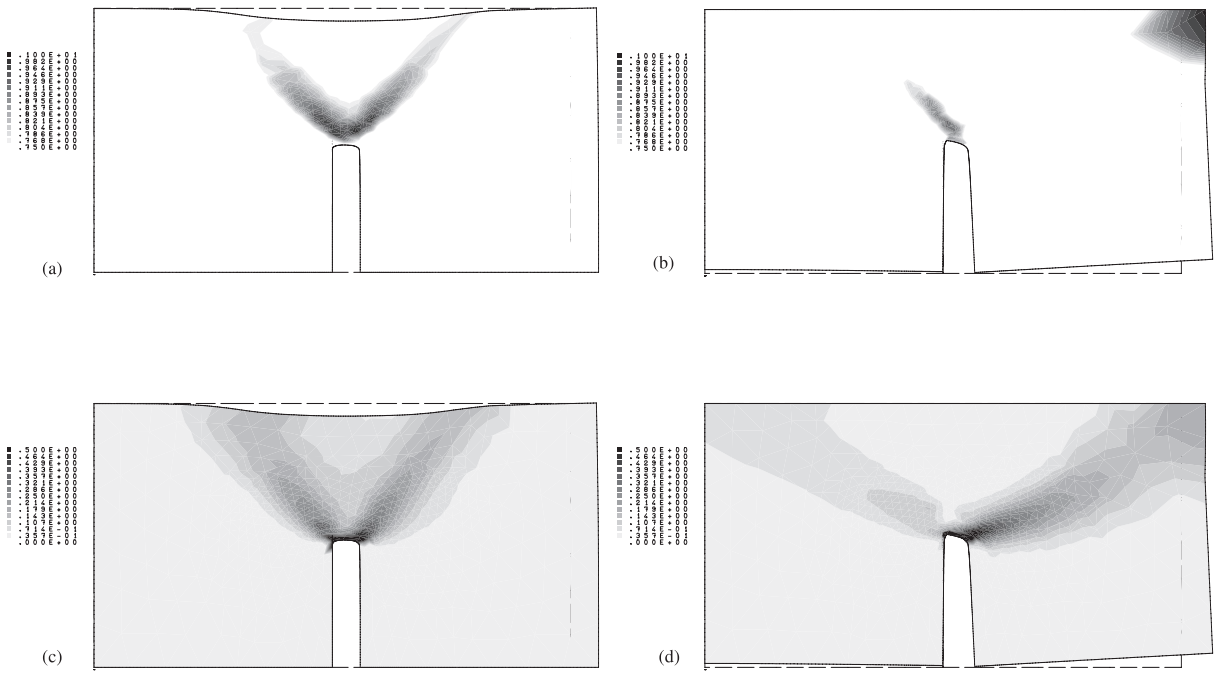

Fig. 8. Creep damage contours: (a) central slit, (b) double edge cracked plate; creep strain contours, (c) central slit, and (d) double edge cracked plate.

double edge cracked plate. These results have shown that the model can predict the patterns of damage evolution within the edge cracked plates.

Finite element computational results have been obtained for notched plates in Bellenger (1998b). Two notched radius have been selected: For the specimen with a sharper tip radius, the damage is highly concentrated at the notch tip region. In the experiments of Ozmat (1991), it was observed that cracks do not continue to grow along the symmetry plane of the blunt notch indefinitely, but eventually show a tendency to bifurcate. A trend in this direction is seen in a later stage of our damage accumulation model. In order to

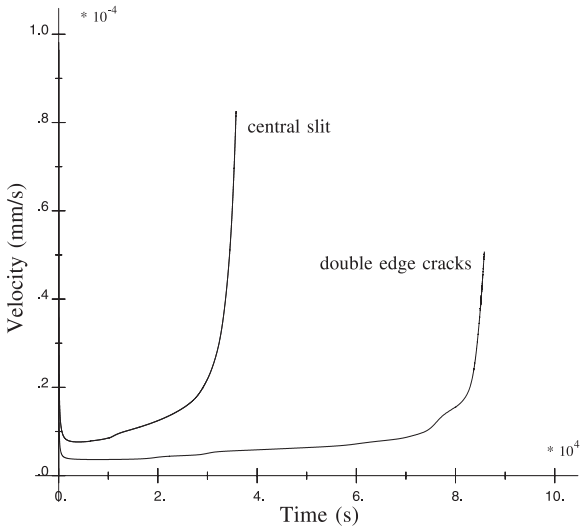

Fig. 9. Creep curves: velocity of the point A (see Fig. 7) for edge cracked plates.

represent another type of notch character, a second geometry with a less sharp tip radius has been selected. The maximum damage starts from the root of the notch and progresses gradually to the centre of the specimen. This is confirmed by the observed appearance of the failed specimen in experimental tests. Furthermore, the specimen with a sharper tip radius has a rupture lifetime in excess of the lifetime of the specimen with a less sharp tip radius for the same average stress level acting on a notch throat. These finite element predictions of rupture times agree well with the experimental rupture times.

4.2.1. Numerical analysis

Numerical results concerning the notched plate with a less sharp tip radius have been obtained with 10 increments for 92% of the loading time (30 000 s). These increments require 14% of the global CPU time. The last 8% of the loading (until 32 500 s) require eight increments and 86% of the global CPU time. Clearly, we can see that the LATIN method can handle large time increments during primary and secondary creep periods to reach swiftly the tertiary creep period. However, if we want an assessment of the creep life, the calculations can be stopped when the tertiary creep period is shown. In this case, we can stop the calculations at 31 000 s and the CPU time is divided by six with a small error on the creep life assessment. If we want to know the post-critical behavior and the damage development until failure, the calculation cost is higher but possible because of the stability of the models which allows us to continue the calculations, in order to describe the tertiary creep period (Bellenger, 1998b). The viscoplastic damage model enables the very different behavior of sharp cracks and notches to be qualitatively described to show the post-critical contours of damage distribution.

4.3. Example 3: L-shaped structure subjected to creep

The above examples used the viscoplastic damage model in nonlinear geometry. For this model, the creep damage increases with time and the geometrical effect is not necessary to describe the tertiary creep period (Fig. 5). However, in order to display a transition zone where the combined ductile–brittle failure mechanism arises, the nonlinear geometrical effect has been introduced.

Now, if we consider that the tertiary creep period arises from ductile phenomena at high stress with a rapid evolution of damage at the end of the creep life, the viscoplastic viscodamage model in nonlinear geometry must be used. Finite element computational results have been obtained for an L-shaped structure using this model. The values of the parameters are given in Table 5. The geometry, the mesh and boundary conditions are shown in Fig. 10.

Unlike the viscoplastic damage model where the geometrical effect was not necessary to have damage evolution (Fig. 5), the viscoplastic viscodamage model requires this geometrical effect. In Fig. 11 the behavior of the model is compared with the model in small perturbations (Curve 1) as well as the behavior of the model in nonlinear geometry without damage ($Z_0 = \infty$) (Curve 2). Clearly, we can see that the tertiary creep description is not possible in small perturbations. This phenomenon arises from the choice of the damage convex defined by the yield function $f_X(Y) \leqslant 0$. Damage occurs only when the state of stress reaches the actual yield function and damage continues to grow if $f_X(Y) > 0$ at each time step. Under a constant applied load, this requires the increase in the stress by the nonlinear geometrical effect. Fig. 12 shows the contours of damage distribution at different creep times. The damage grows swiftly by creep deformation at the end of the creep life, to produce a more pronounced tertiary creep phase.

This example using the viscoplastic viscodamage model in nonlinear geometry has shown a ductile fracture preceded by a reduction in the cross-sectional area due to large creep strains, damage subsequently grows further by creep deformation.

4.4. Example 4: simplified study of turbine casing

Creep strains and damage development in simplified turbine casting (Fig. 13) under steady loads (pressure) (Dawson et al., 1980) have been predicted using the above models in order to display on the same structure different crack growth behaviors and their dependences on the stress levels. We will take one quarter of the structure: the geometry, the loading and boundary conditions are shown in Fig. 13. The values of the parameters used in the viscoplastic (visco) damage models are given in Tables 6 and 7. For viscoplastic behavior the parameters correspond to stainless steel 17–12 SPH at 600°C.

To describe a ductile fracture phenomenon with the viscoplastic viscodamage model in nonlinear geometry, a loading of 12 MPa is applied. In this case, damage initially appears in zone B (Fig. 14(b)) followed by necking in zone C and damage appearance in this zone by creep deformation (Fig. 14(b)). Nevertheless, the ductile rupture mechanism occurs in zone C, because the damage level is more important than in zone B. This ductile phenomenon results from large creep strains. The geometrical effect can be seen in Fig. 15(b), which shows the creep strain contours. The creep curve which gives the displacement of point A

Table 5
Summary of material parameters for the L-shaped structure

Parameters	
E (MPa)	50 000
v	0.3
n	5
K	1200
R_0	150
Q	10
b	500
Z_0	0.4
A	25

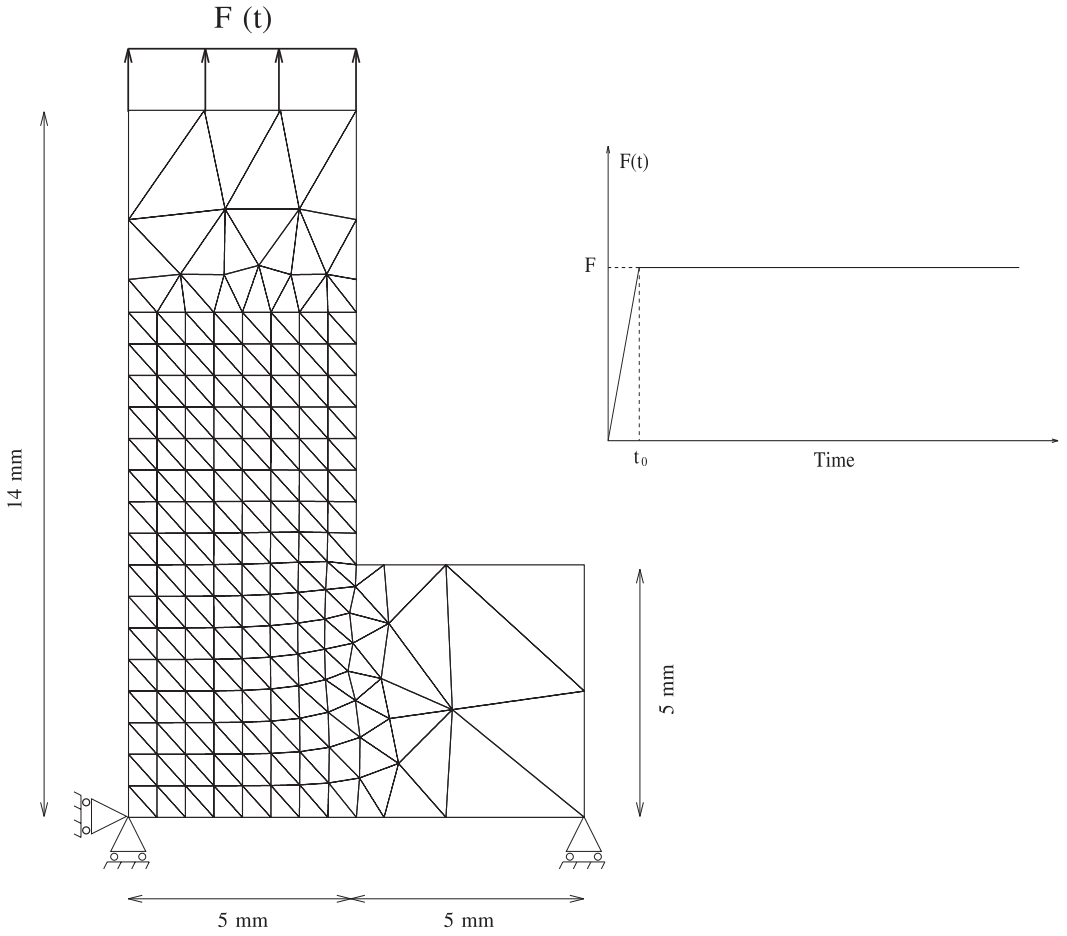

Fig. 10. Geometry, mesh, boundary conditions and loading of the L-shaped structure ($F = 220$ MPa).

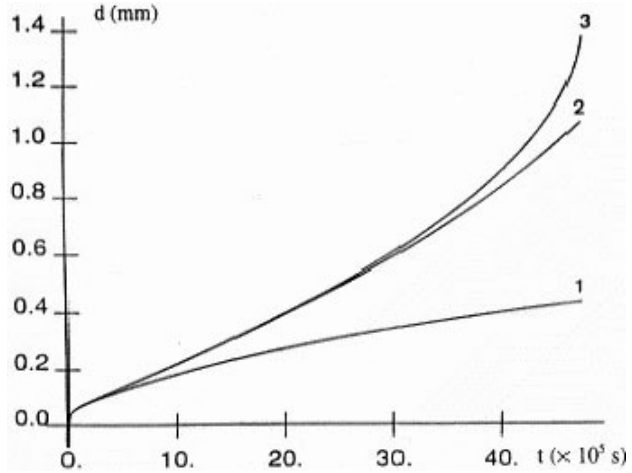

Fig. 11. Creep curves – displacement with time of the loaded extremity for the L-shaped structure: 1. viscoplastic viscodamage model in small perturbations, 2. viscoplastic model in nonlinear geometry and 3. viscoplastic viscodamage model in nonlinear geometry.

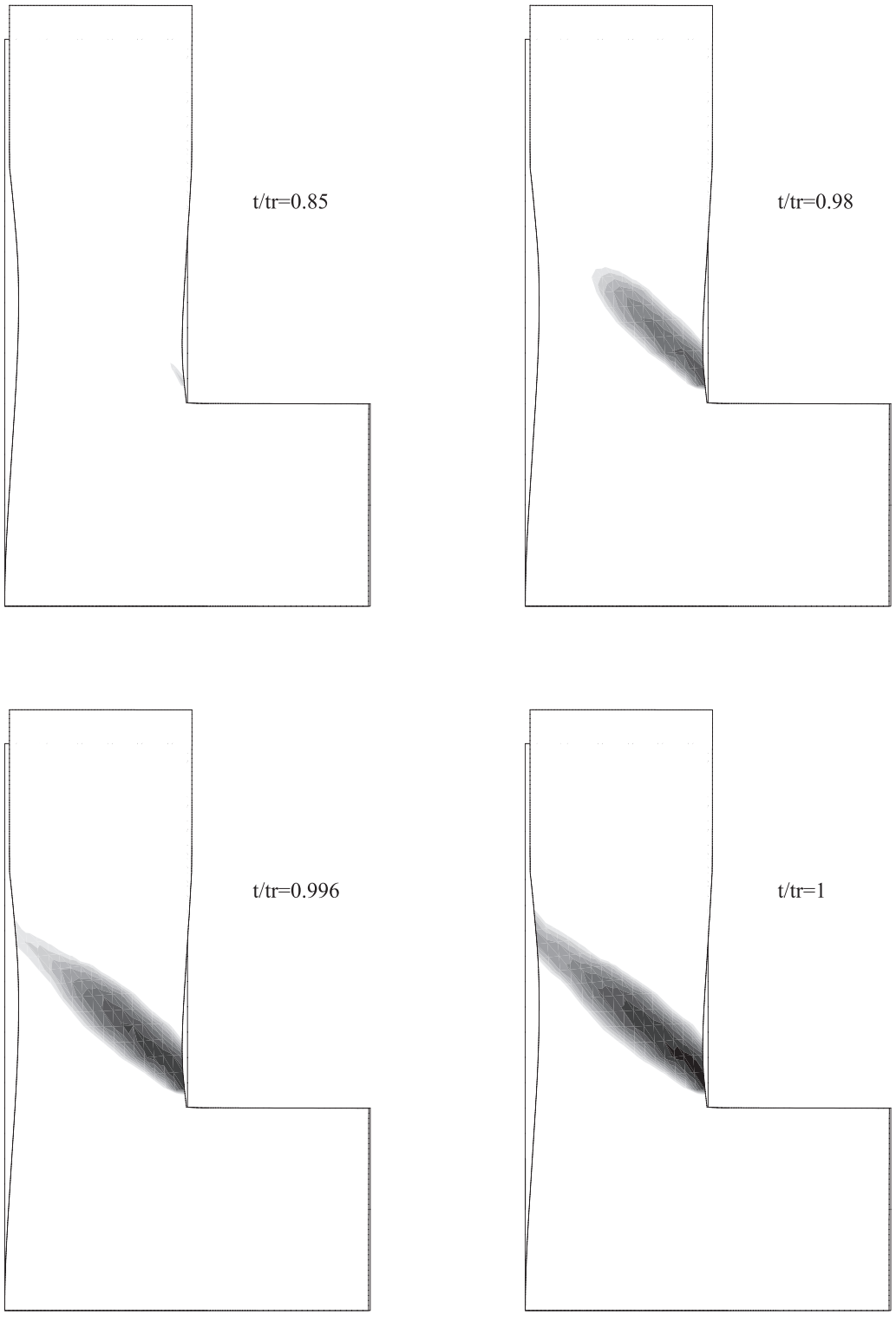

Fig. 12. Creep damage contours at different creep times (t_r = rupture time).

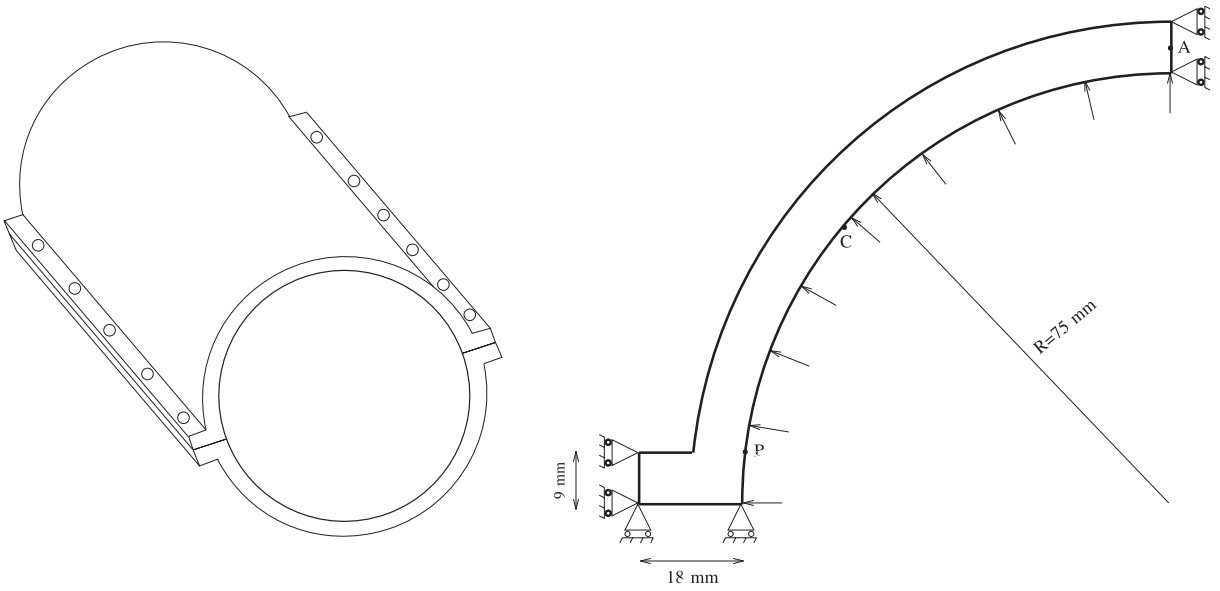

Fig. 13. Simplified turbine casing, geometry and boundary conditions.

Table 6
Summary of material parameters for the simplified turbine casing

17–12 SPH 600°C						
n	K	Q	b	R_0	E (MPa)	v
12	150	80	10	6	145 000	0.3

Table 7
Summary of damage material parameters for the simplified turbine casing

Viscoplastic damage model				Viscoplastic viscodamage model	
n_x	q	c	Z_0	Z_0	A
3	0.5	0.038	0	0.04	100

with time (Fig. 16(a)) shows a pronounced tertiary creep phase which allows us to obtain a creep life assessment.

In order to describe a brittle, but much more creep resistant fracture morphology, a loading of 6 MPa is applied using the viscoplastic damage model in non linear geometry. Fig. 14(a) shows the contours of damage distribution at different creep times. It is clear that the damage is concentrated at the inner surface of the shoulder. In this zone, damage reaches values superior to 99.9%. At rupture, the Von Mises stress reaches zero for the most damaged point (point B) (Fig. 16(b)) when the stress for point C remains constant throughout loading. This calculation describes a brittle fracture caused by the deterioration of material with time. This mechanism occurs at low stress levels. The overall geometric effect is not observed since

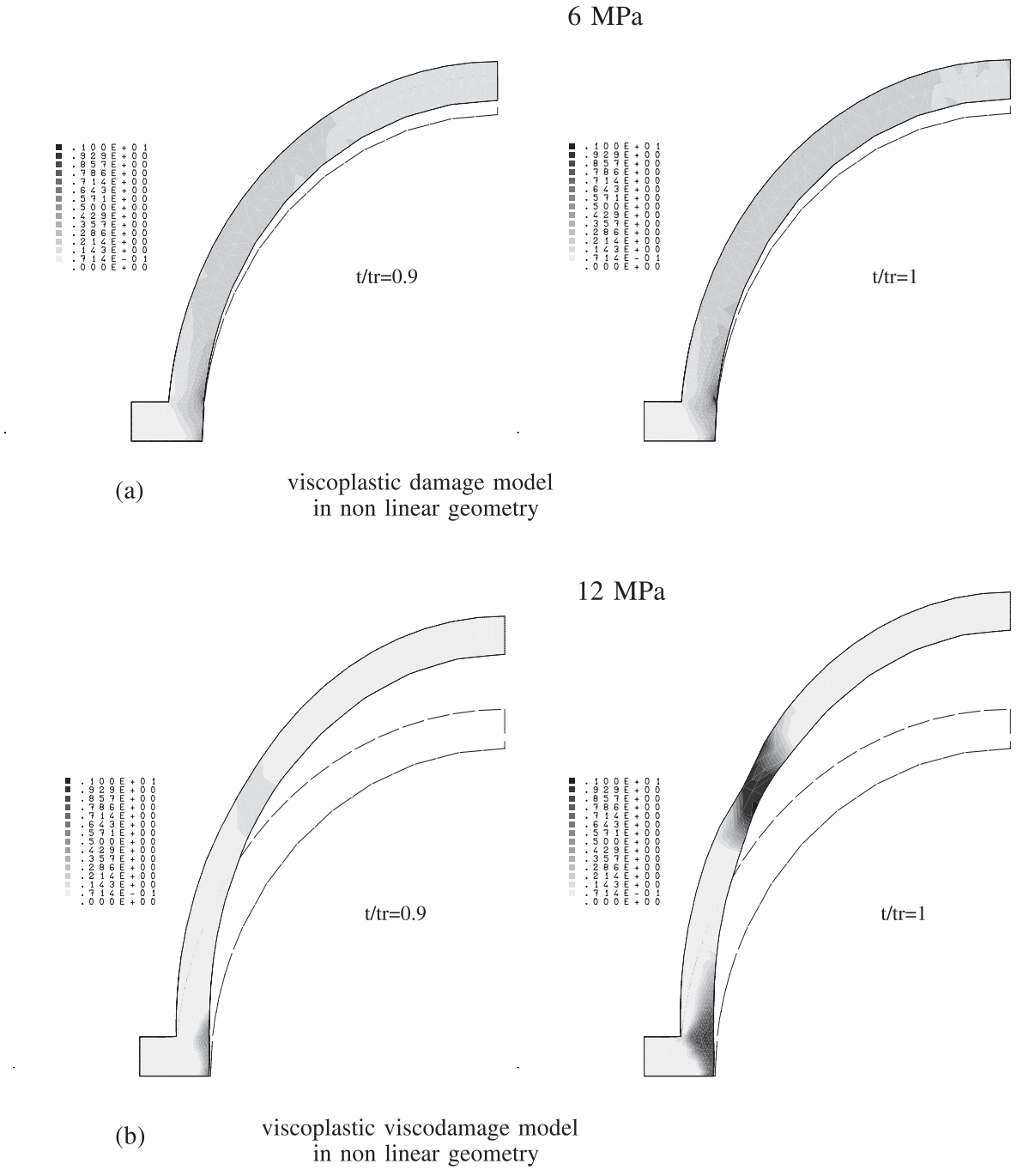

Fig. 14. Creep damage contours at different creep times (t_r = rupture time).

creep strains are small (Fig. 15(a)) and the lifetime is much higher: 316 500 s (3600 s for the loading of 12 MPa).

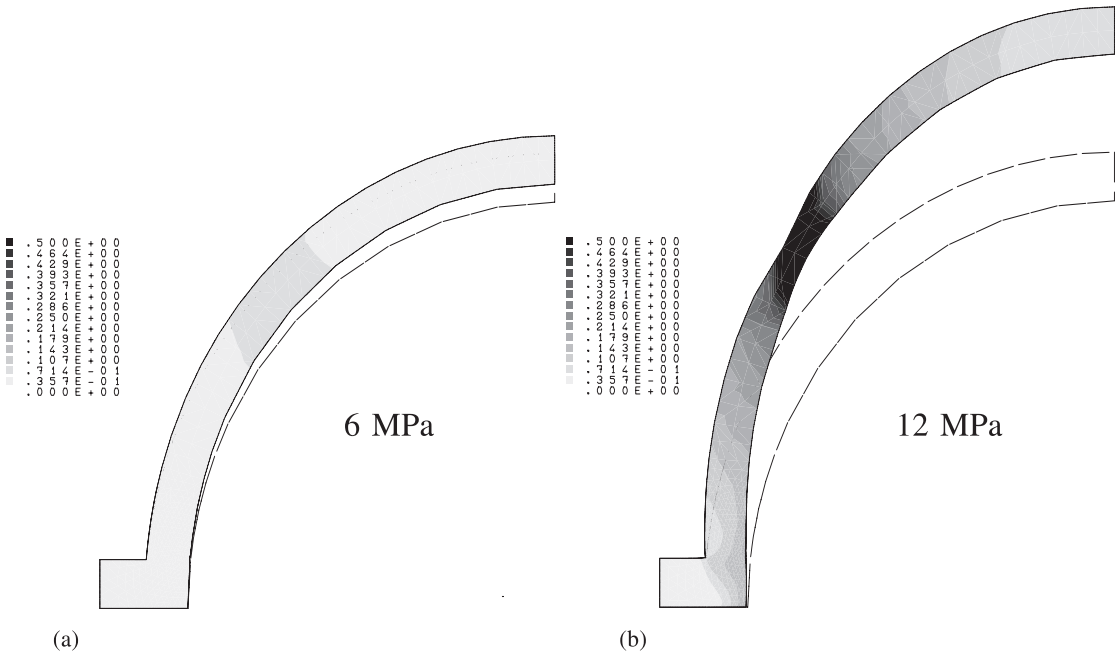

Fig. 15. Creep strain contours at $t/\mathrm{tr} = 1$.

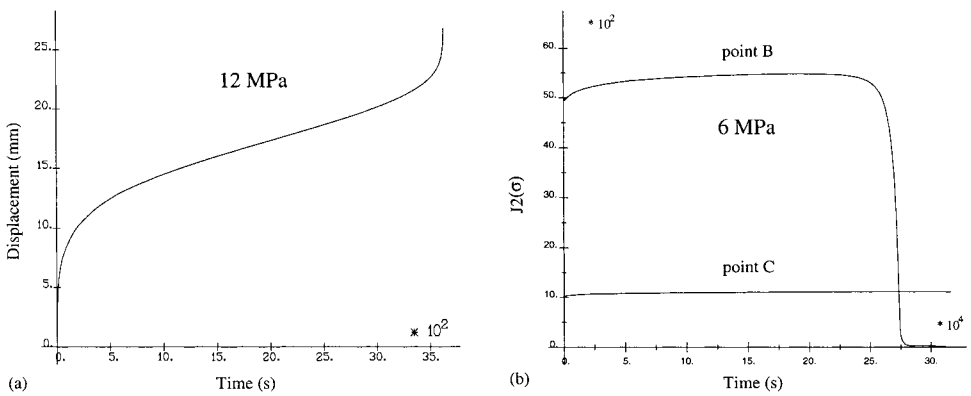

Fig. 16. (a) Displacement with time of the point A (see Fig. 13) with a loading of 12 MPa; (b) Local evolutions with time of the Von Mises equivalent stress (loading of 6 MPa).

5. Conclusions

In this paper, a macroscopic modeling of creep behavior has been proposed. Backstress models within unified formulation have been used for numerical simulations of primary and secondary creep periods, associated with a scalar damage variable and nonlinear geometrical effects for tertiary creep description. Two damage models have been introduced in order to describe different modes of creep damage evolution. Numerical examples have shown that the proposed approach can describe these different failure mecha-

nisms with an accurate prediction of the patterns of damage evolution for a large range of components. Furthermore, the numerical properties of the models allow us to obtain a different crack growth development, in order to know the post-critical behavior and the damage development until failure. We have proposed to use the LATIN method in a version adapted to solve problems with geometrical nonlinearities. This method describes primary and secondary creep periods in a few large time increments to reach swiftly the tertiary creep period. If creep life assessment or creep strains evolution are the aims of a study, the LATIN method allows us to obtain a rapid solution to the problem in a few time increments (one increment for uniaxial creep problem). In this case, we can stop the calculations when the tertiary creep period is displayed, with a small error on the creep life assessment. If we want to know the post-critical behavior, the calculations are possible because of the stability of the models, which allow us to continue these calculations in order to describe the tertiary creep period.

References

Abdali, A., Benkrid, K., Bussy, P., 1996. Simulation of sheet metal cutting by the large time increment method. J. Mater. Process. Technol. 60, 255–260.

Argon, A.S., 1982. Mechanics and mechanisms of fracture in creeping alloys. In: Recent Advances in Creep and Fracture of Engineering Materials and Structures. Pineridge Press, Swansea.

Bellenger, E., Bussy, P., 1998a. Plastic and viscoplastic damage models with numerical treatment for metal forming processes. J. Mater. Process. Technol. 80, 591–596.

Bellenger, E., 1998b. Modélisation et simulation numérique du fluage des structures viscoplastiques endommageables. Thèse de Doctorat d'Université, Amiens.

Benkrid, K., Bussy, P., Abdali, A., 1994a. On the stable damage model for metal forming processes. J. Mater. Process. Technol. 45, 521–526.

Benkrid, K., 1994b. Simulation numérique des procédés de mise en forme: Analyse de l'endommagement. Thèse de Doctorat d'Université, Amiens.

Boisse, P., Bussy, P., Ladevéze, P., 1990. A new approach in nonlinear mechanics: the large time increment method. Int. J. Num. Meth. Engng. 29, 647–663.

Bussy, P., Liu, B., Vauchez, P., 1990. Numerical simulation of metal forming processes: the large time increment method. In: Proceedings of the Second World Congress on Computational Mechanics. Stuttgart.

Chaboche, J.L., Nouailhas, D., 1989. A unified constitutive model for cyclic viscoplasticity and its applications to various stainless steels. J. Engng. Mater. Technol. ASME 111, 424.

Chen, I.W., Argon, A.S., 1981. Creep cavitation in 304 stainless steel. Acta Meta. 29, 1321.

Dawson, J.J., Fessler, H., Hyde, T.H., Webster, J.J., 1980. Elasto plastic creep behaviour of axially loaded shouldered tubes. J. Strain Anal. 15, 21–29.

Don, J., Majumbar, S., 1986. Creep cavitation and grain boundary structure in type 304 stainless steel. Acta Meta. 34, 961.

Germain, F., 1972. Cours de mécanique des milieux continus. Masson et Cie, Paris.

Halphen, B., Nguyen, Q.S., 1975. Sur les matériaux standards généralisés. J. Méca. 14, 39–63.

Harrison, G.F., Homewood, T., 1994. The application of the Graham Walles creep equation to aeroengine superalloys. J. Strain Anal. 29(3).

Holcomb, D.J., Costin, L.S., 1986. Detecting damage surface in brittle materials using acoustic emissions. J. Appl. Mech., ASME 53, 536–544.

Kachanov, L.M., 1958. Time to rupture process under creep conditions. Izv. Akad. Nauk. USSR, Otd. Tekh. Nauk 8. 26–31.

Krajcinovic, D., 1989. Damage mechanics. Mech. Mater. 8, 127.

Ladevèze, P., 1981. Sur la thèorie de la plasticité en grandes déformations. Rapport interne No. 9, L.M.T Cachan.

Ladevèze, P., 1985. Sur une famille d'algorithmes en mecanique des structures. C.R., Acad. des Sc., Série II, 300(2), 317–365.

Leckie, F.A., Hayhurst, D.R., 1977. Constitutive equations for creep rupture. Acta Meta. 25, 1059.

Lemaitre, J., Chaboche, J.L., 1978. Aspects phénomènologiques de la rupture par endommagement. Journal de Mécanique Appliquée 2(3).

Lemaitre, J., 1984. How to use damage mechanics. Nucl. Engng. Design 80, 233.

Lemaitre, J., Chaboche, J.L., 1985. Mécanique des matériaux solides. Dunod, Paris.

Murakami, S., Ohno, N., 1988. Continuum theory of material damage at high temperature. In: Ohtani, et al. (Eds.), High Temperature Creep Fatigue. Elsevier, Amsterdam, p. 43.

Ortiz, M., Simo, J.C., 1986. An analysis of a new class of integration algorithms for elastoplastic constitutive relations. Int. J. Num. Meth. Engng. 23, 353–366.
Ozmat, B., 1991. Growth modes of cracks in type 304 stainless steel. Mech. Mater. 11, 1.
Rabotnov, Y.N., 1968. Creep rupture. In: Proceedings of the 12th International Congress on Applied Mechanics. Springer, Standford.
Rice, J.R., 1970. On the structure of stress–strain relations for time dependent plastic deformation in metals. J. Appl. Mech., ASME 37, 728–737.
Riedel, H., 1987. Fracture at high temperatures. Appl. Mech., ASME 37, 728–737.
Robinson, D.N., 1978. A unified creep-plasticity model for structural metals at high temperatures. Oak Ridge National Laboratory, TM 5969.
Rougée, P., 1991. A new Lagrangian intrinsic approach to large deformations in continuous media. Eur. J. Mech. A/Solids 10, 15–39.
Saanouni, K., Chaboche, J.L., Bathias, C., 1986. On the creep crack growth prediction by a local approach. Engng. Fract. Mech. 25, 677.
Skrzypek, J.J., 1993. Plasticity and Creep, Theory, Examples and Problems. CRC Press, Boca-Raton, FL.
Tvergaard, V., 1985. Analysis of creep rupture in a notched tensile bar. Mech. Mater. 4, 181.
Wilshire, B., Evans, R.W., 1994. Acquisition and analysis of creep data. J. Strain Anal. 29(3).